The dyslexia susceptibility gene KIAA0319 influences cilia length, cell migration and mechanical cell-substrate interaction

Rebeca Diaz[*,1], Nils M. Kronenberg[*,2], Angela Martinelli[1], Philipp Liehm[2], Andrew C. Riches[1], Malte C. Gather[2], Silvia Paracchini[1].

* These authors have contributed equally to this paper

[1] School of Medicine, University of St Andrews, St Andrews, KY16 9TF, UK

[2] SUPA, School of Physics and Astronomy, University of St Andrews, St Andrews, KY16 9SS, UK

Corresponding authors:

Silvia Paracchini sp58@st-andrews.ac.uk

Malte Gather mcg6@st-andrews.ac.uk

Keywords

KIAA0319, neurodevelopment, dyslexia, cilia, podosomes, cytoskeleton, CRISPR, force microscopy, mechanobiology

Abstract

Dyslexia is a common neurodevelopmental disorder with a strong genetic component. Independent genetic association studies have implicated the *KIAA0319* gene in dyslexia, however its function is still unknown.

We developed a cellular knockout model for KIAA0319 in RPE1 cells via CRISPR-Cas9n to investigate its role in processes suggested but not confirmed in previous studies, including cilia formation and cell migration.

We found that KIAA0319 knockout increased cilia length and accelerated cell migration. Using Elastic Resonator Interference Stress Microscopy (ERISM), we detected an increase in cellular force for the knockout cells that was restored by a rescue experiment. Combining ERISM and immunostaining showed that KIAA0319 depletion reduced the number of podosomes formed by the cells.

Our results suggest an involvement of KIAA0319 in mechanosensing and force regulation and shows for the first time that podosomes exert highly dynamic, piconewton vertical forces in epithelial cells.

Introduction

Dyslexia is a neurodevelopmental disorder that affects around 5% of school-aged children and refers to unexpected difficulties in learning to read (Peterson & Pennington, 2012). In spite of the high heritability of dyslexia (up to 70%), very few candidate genes have been identified so far (Paracchini et al., 2016). Among those, *DYX1C1*, *DCDC2*, *ROBO1* and *KIAA0319* are supported by independent, family-based association studies and have been investigated at functional level (Newbury et al., 2014; Paracchini et al., 2016). Initial *in utero* gene silencing experiments in rats for these genes provided strong support for the neuronal migration hypothesis (Paracchini et al., 2007) first proposed in the eighties (Galaburda et al., 1985). This hypothesis is based on the observation of subtle cortical anomalies, i.e. heteropias and microgyrias, in post-mortem brains from individuals with dyslexia (n = 8). Such anomalies are likely to be the result of neuronal migration defects. However, knockout mouse models for DYX1C1, DCDC2 and KIAA0319 did not present cortical alterations (Martinez-Garay et al., 2016; Rendall et al., 2015; Wang et al., 2011). Instead, some of the knockouts for these genes showed defects in auditory processing (Guidi et al., 2017; Truong et al., 2014). These results are consistent with defects in auditory processing underlying dyslexia (Tallal, 1980). Speech sound processing deficits were also described in adult rats that underwent either *Kiaa0319* or *Dyx1c1* silencing during embryonic development (Centanni, Booker, et al., 2014; Centanni, Chen, et al., 2014; Szalkowski et al., 2012; Threlkeld et al., 2007). Explanations for the discordance between knockdown experiments in rat and knockout mouse models included species-specific effects, compensatory mechanisms in mouse, or artefacts in shRNA experiments (Baek et al., 2014; Rossi et al., 2015). The discordance has also led to extensive reviews of the literature and to revisit the neuronal migration hypothesis (Galaburda, 2018; Guidi et al., 2018).

In parallel, new roles for DCDC2, DYX1C1, ROBO1 and KIAA0319 have been described in cilia biology (Paracchini et al., 2016). Transcriptomic studies showed differential expression for these genes in ciliated tissue (Geremek et al., 2014; Hoh et al., 2012; Ivliev et al., 2012). Beyond these studies, a role of KIAA0319 in cilia biology for has not been described yet, but cellular and animal DCDC2 and DYX1C1 knockouts presented cilia defects (Chandrasekar et al., 2013; Grati et al., 2015; Massinen et al., 2011; Schueler et al., 2015; Tarkar et al., 2013), and ROBO1 has

been shown to localize to the cilium of mouse embryonic interneurons (Higginbotham et al., 2012). Mutations in DYX1C1 and DCDC2 have been identified in patients with ciliopathies, a group of disorders caused by defective cilia and often characterised by alterations in body asymmetry (Massinen et al., 2011; Schueler et al., 2015; Tarkar et al., 2013). DCDC2 stabilizes the microtubules in the axoneme, and its overexpression causes elongation of the primary cilium. Lower numbers of cilia and atypical cilia length are common indicators of defects at this cellular structure, and have been implicated in developmental defects, such as craniofacial abnormalities and malformation of the CNS (Avasthi & Marshall, 2012). Cilia length is regulated by the interplay between actin depolymerisation and stabilisation in a tightly regulated process; however, the exact underlying regulation and involved proteins remain to be fully explained (Avasthi & Marshall, 2012). Cilia biology has been proposed as a molecular link to explain the atypical brain asymmetries which are consistently reported for neurodevelopmental disorders, such as dyslexia (Brandler & Paracchini, 2013). However, KIAA0319 cellular function remains largely uncharacterised and most of what is known about this gene has been described through over-expression and knock-down experiments in human cell lines and in animal models. KIAA0319 has been shown to undergo proteolytic processing, with a possible subsequent role in signalling pathways (Velayos-Baeza et al., 2010), and inhibits axon growth (Franquinho et al., 2017). A gene expression analysis in zebrafish showed very high expression in the first hours of development and specific signal in defined embryonic structures, including the notochord and the developing eye and optic vesicles (Gostic et al., 2019). KIAA0319 encodes a transmembrane protein with five PKD domains (Velayos-Baeza et al., 2007) (Figure 1A). Such structures have been previously found in cell surface proteins and are known to be involved in cell-cell and cell-matrix interactions (Bycroft et al., 1999; Hughes et al., 1995; Ibraghimov-Beskrovnaya et al., 2000).

With this work, we seek to shed light on the role of KIAA0319 in cilia formation and as a regulator of mechanical forces during cell migration. We generated the first cellular knockout model of KIAA0319 in human cells to specifically investigate its role in cilia biology and neuronal migration, addressing the two main hypotheses currently proposed. We used retina pigmented epithelium cells (RPE1), which are particularly suitable to study cilia (Kim et al., 2015; Pugacheva et al., 2007), and studied their mechanobiology using the recently introduced Elastic Resonator Interference Stress

Microscopy (ERISM) (Kronenberg et al., 2017). ERISM allows for continuous imaging of cell forces with high spatial resolution and over extended periods of time. This is achieved by growing cells on a substrate that consists of a layer of an ultra-soft elastomer situated between two semi-transparent, mechanically flexible gold mirrors, which form an optical micro-cavity. Mechanical force and stress exerted by cells cause local deformations of this micro-cavity and thus local shifts to its resonance wavelengths. The resulting interference patterns are analysed by optical modelling in order to compute a high-resolution displacement map with µm lateral resolution and nm vertical displacement resolution (Liehm et al., 2018), which allows for the detection of forces in the Piconewton range. Unlike many other stress microscopy techniques, ERISM does not require a zero-stress reference image, so cells can be kept on the substrate for time-lapse imaging and immunostaining. The low probe light intensity and mechanical stability of the micro-cavity substrate enable long-term measurements of cell forces without phototoxic effects or mechanical degradation of the substrate.

Our data show that loss of KIAA0319 in RPE1 cells leads to the formation of longer cilia and to an increase in cellular force. The force phenotype of the wild type was rescued by expressing a KIAA0319-GFP fusion construct in the knockout cells. Our data further indicate that KIAA0319 knockout cells form fewer podosomes, a special type of cell-matrix contact that in the past been has shown to have mechanosensitive function (Labernadie et al., 2014). Using ERISM we were able to show that these podosomes exert oscillating, vertical forces, possibly for mechanical probing of the substrate. Our measurements present the first observation of mechanical activity of podosomes in epithelial cells. The results of this study show that KIAA0319 knockout strongly affects the mechanical phenotype of RPE1 cells and suggest a function of KIAA0319 in mechanosensing and force regulation.

Results

Generation of KIAA0319 KO in RPE1 cell lines

We generated a KIAA0319 knockout model in RPE1 cells by introducing random modifications in exon 6 with CRISPR-Cas9n based genome editing. The *KIAA0319* main isoform (NM_014809) consists of 21 exons and spans 102 kb of human chromosome 6 (Figure 1A). We generated a biallelic knockout (Ex6KO) by causing deletions that introduce premature stop codons in the reading frame of *KIAA0319*

using paired gRNAs (Figure 1B). The deletion was confirmed by RT-PCR (Figure 1C). Transcript quantification by qRT-PCR shows that KIAA0319 expression in Ex6KO is five-times lower than the wild-type (*t*-test, $p < 0.001$) consistently with nonsense-mediated decay (Baker & Parker, 2004) (Figure 1D).

KIAA0319 knockout cells form longer cilia

For assessment of KIAA0319 involvement in cilia formation, cilia length in RPE1 wild type (WT) and Ex6KO cells were measured by staining of the cilium-specific protein ARL13B and analysis of epi-fluorescence images (Figure 2A & B). While a similar fraction of WT and Ex6KO cells formed cilia (WT: 379/571, 68%; Ex6KO: 271/383, 70%), the cilia in Ex6KO were significantly longer than in the wild type (mean ± SEM: WT: 4.5 µm ± 0.1 µm, $n = 129$; Ex6KO: 6.1 µm ± 0.2 µm, $n = 104$; *t*-test: $p < 0.001$; Figure 2C).

Cell morphology, migration speed and force exertion are altered in KIAA0319 knockout cells

We performed a scratch assay on a confluent layer of cells to test collective cell migration. This assay did not reveal a significant difference between the collective migratory speed of WT and Ex6KO cells after 24 h (mean cell coverage ± SEM: WT: 27.4% ± 4.2%, $n = 3$; Ex6KO: 30.2% ± 3.5%, $n = 3$; *t*-test: $p = 0.63$; Supplementary Figure 1).

Next, we tested the migration of single cells. WT and Ex6KO cells were plated on ERISM substrates with an effective stiffness of 6 kPa at a density low enough to ensure non-confluency and thus allow mapping of the forces exerted by individual cells (Figure 3A). Ex6KO cells covered a smaller surface area than WT cells (mean cell area ± SEM: WT: 2052 µm^2 ± 91 µm^2, $n = 36$; Ex6KO: 1295 µm^2 ± 65 µm^2, $n = 36$; *t*-test: $p < 0.001$; Figure 3B), even though the shape and morphology of the cells did not differ. The displacement maps recorded with ERISM (Figure 3A) revealed that cells from both lines exert similar force patterns on their substrate: pulling was focused around the two long ends of the cells, perpendicular to the direction of migration (cells were polarised in a way that the nucleus was positioned posterior to the direction of migration). Downward compression was observed underneath the centre of the cells. This displacement pattern is a fingerprint for the exertion of

contractile forces by adherent cells (Kronenberg et al., 2017). (See next section for discussion of the other features in the ERISM map).

The migratory behaviour and the associated dynamics of force exertion of WT and Ex6KO cells were then investigated by taking time-lapse measurements of phase contrast and ERISM displacement maps in five-minute intervals over a time span of 17 hours (Supplementary Movie 1 & 2). The average speed of single cell migration was significantly higher for Ex6KO than for WT cells (mean speed ± SEM: WT: 0.33 µm min^{-1} ± 0.03 µm min^{-1}, n = 10; Ex6KO: 0.44 µm min^{-1} ± 0.04 µm min^{-1}, n = 13, t-test: p = 0.04; Figure 3C). This result contrasted with the results from the scratch assay for collective cell migration (Supplementary Figure 1). The directness of the migration was not affected by the KIAA0319 knockout (Supplementary Figure 2A).

To assess the mechanical activity of cells, we compute the total volume by which each cell indents into the substrate and use this as a proxy for the applied force. Comparing the temporal averages of applied force during migration shows that Ex6KO cells exert significant stronger contractile forces on the substrate than WT cells (mean indented volume ± SEM: WT: 167 $µm^3$ ± 19 $µm^3$, n = 10; Ex6KO: 319 $µm^3$ ± 39 $µm^3$, n = 13; t-test: p = 0.004, Figure 3D). Figure 3E summarizes the temporal evolution of migratory speed and applied force for a representative WT and Ex6KO cell, respectively. The Ex6KO cell showed more pronounced fluctuations in speed and applied force than the WT cell.

To analyse the temporal evolution of mechanical activity in more detail, we computed the temporal Fourier transform of the data. This revealed that the mean amplitude of oscillations in both migratory speed and applied force is larger for Ex6KO cells than for WT cells (amplitude of oscillations in migratory speed increased by mean factor of 1.4 over the analysed frequency range; amplitude of oscillations in indented volume increased by mean factor of 1.5 over the analysed frequency range; WT: n = 11, Ex6KO: n = 13; Supplementary Figure 2B & C). However, neither of the two oscillation amplitudes were increased at a statistically significant level (mean amplitude of oscillation in migration speed: t-test: p = 0.06 – 0.54; mean amplitude of oscillation in indented volume: t-test: p = 0.16 – 0.49). The time traces in Fig. 3E also show that for the Ex6KO cell occasional single events of high migration speed were correlated with a drop in exerted force (indicated by red, vertical lines).

To validate our findings of the impact of KIAA0319 on cell force exertion, we conducted a rescue experiment by generating an Ex6KO cell line with stable expression of KIAA0319-GFP fusion protein (Ex6KO K-GFP; Figure 4A). We also generated a control line of RPE1 WT cells with the same construct (WT K-GFP). Even though the KIAA0319 rescue did not recover the reduction in cell area seen for Ex6KO cells [mean cell area ± SEM: WT: 2315 μm^2 ± 200 μm^2, n = 16; WT K-GFP: 2299 μm^2 ± 107 μm^2, n = 20; Ex6KO: 1565 μm^2 ± 123 μm^2, n = 23; Ex6KO K-GFP: 1297 μm^2 ± 131 μm^2, n = 17; Figure 4B], the level of cell force was restored in Ex6KO K-GFP cells [mean indented volume ± SEM: WT: 115 μm^3 ± 14 μm^3, n = 16; WT K-GFP: 96 ± 9 μm^3, n = 19; Ex6KO: 186 ± 20 μm^3, n = 24; Ex6KO K-GFP: 125 ± 16 μm^3, n = 16; t-test(WT vs. Ex6KO): p = 0.01, t-test(WT vs. Ex6KO K-GFP): p = 0.67; Figure 4C)].

RPE1 KIAA0319 WT and Ex6KO show different fine patterns of force exertion

Given the differences in cilia length, cell size, migration speed and exerted force we reasoned that KIAA0319 knockout might affect cytoskeleton dynamics. To test this hypothesis, we took phase contrast and ERISM time-lapse measurements of migrating WT and Ex6KO cells at 5 seconds intervals (Supplementary Movie 3 & 4), and fixed and immunostained the cells for actin and vinculin immediately after the time-lapse. Spatial Fourier-filtering of ERISM maps can be used to filter out broad deformation features associated with the overall contractility of cells and thus resolve finer details linked to interaction of sub-cellular components, e.g. focal adhesions or podosomes, with the substrate (Kronenberg et al., 2017). (For further discussion on the displacement fine-structure in Fourier-filtered displacement maps see Supplementary Figure 3.) Figure 5A shows phase contrast images, Fourier-filtered ERISM maps and immunofluorescence microscopy images for a WT and Ex6KO cell. The Fourier-filtered displacement maps of both cells show small push-pull features that co-localised with vinculin-rich areas in the immunofluorescence microscopy images. Insets ii) and iii) in Figure 5A highlight examples of such areas for the WT and the Ex6KO cell, respectively. Vinculin is enriched in the centre between pulling (red areas in Fourier-filtered ERISM maps) and pushing (green areas), and actin fibres are connected to vinculin on the pulling site. Push-pull features in Fourier-filtered ERISM maps were previously attributed to focal adhesions transmitting contractile, mostly horizontal forces to the substrate that are generated by the actin cytoskeleton

(Kronenberg et al., 2017). In agreement with these earlier observations, in the Ex6KO cell, the axes defined by the push-pull features co-aligned with the actin fibres that connect different vinculin-rich sites (see Figure 5A and Supplementary Figure 3). This push-pull behaviour is also consistent with earlier observations of torque being applied by focal adhesions (Legant et al., 2013). Since the formation and alignment of stress fibres is less distinct in the WT cell, the above-mentioned co-alignment of actin, vinculin and the ERISM push-pull features is also less pronounced for the WT cell. In agreement with this, the forces exerted by single focal adhesions are smaller in the WT cell (Figure 5C & D).

Beside focal adhesions, the Fourier-filtered ERISM displacement map of the WT cell also showed tightly confined pushing sites with a diameter of about 2 µm (green-blue areas highlighted with black arrow heads in Fourier-filtered ERISM map of Figure 5A). These pushing sites were surrounded by circularly arranged dots of upward pulling (red areas). Immunocytochemistry analysis showed that the pushing sites corresponded to actin-rich locations (white arrow heads in epi-fluorescence image of Figure 5A), whereas pulling around the pushing sites colocalised with vinculin-rich positions (in inset i) in Figure 5A). This protein arrangement is a hallmark for podosomes, a cellular adhesion structure that is chiefly formed in monocyte-derived cells (Linder & Wiesner, 2016) but that has also been reported in spreading and migrating epithelia cells (Spinardi et al., 2004).

The time-lapse measurement revealed that the podosomes exerted an oscillating vertical force, that reached maximum values of up to 80 pN (Figure 5B). The horizontal contractile forces exerted by focal adhesions were roughly 100-times larger than the vertical indentation forces exerted by podosomes (Figure 5B & D). However, while podosomal pushing was highly dynamic, the horizontal forces originating from focal adhesions were relatively static and showed little oscillation in force. Focal adhesions at the leading edge of the cell were chiefly stationary once assembled (top right in Supplementary Movie 4) and any lateral movement of focal adhesions was confined to the trailing edge of the cell (bottom left in Supplementary Movie 4).

The WT and Ex6KO cell shown in Figure 5 and Supplementary Movie 3 & 4 are examples illustrating the general differences between the two force transmission patterns (podosomes and focal adhesion). In total, combined ERISM and

immunochemistry measurements were carried out for 33 cells (see Supplementary Figure 4 and Supplementary Movie 5 & 6 for further examples). While both WT and Ex6KO cells form podosomes (Supplementary Figure 4), their prevalence was higher in WT cells; while 63% of the investigated WT cells formed podosomes (10 out of 16), they were only observed in 18% of Ex6KO cells (3 out of 17).

Discussion

We successfully developed a cellular knockout model via CRISPR-Cas9n to study the potential role of the *KIAA0319* gene in cilia biology and cell migration. Sequencing confirmed loss-of-function deletions in the sixth exon of KIAA0319 and qRT-PCR analysis showed a strong decrease in the expression of KIAA0319, consistent with nonsense mediated decay of the transcript (Figure 1). We set out to characterise this cellular model to investigate specifically the role of KIAA0319 in cilia biology and neuronal migration on the basis of the dominating hypothesis proposed by the literature (Paracchini et al., 2016) .

Although the same fraction of KIAA0319 Ex6KO and WT cells developed cilia, these were significantly longer in the knockout (Figure 2C). Cilia biology is emerging as a contributing factor to a range of diseases, including neurodevelopmental disorders and dyslexia (Paracchini et al., 2016). Other dyslexia candidate genes have been reported to affect cilia length. DYX1C1 knockouts present shorter cilia than the wild type in zebrafish (Chandrasekar et al., 2013), and overexpression of DCDC2 increases cilia length in rat neurons (Massinen et al., 2011). The only evidence in support of a role of KIAA0319 in cilia comes from transcriptomic studies (Geremek et al., 2014; Hoh et al., 2012; Ivliev et al., 2012). Our work is therefore the first study to support a role for KIAA0319 in cilia biology in a biological model. In turn, these data further support the role of cilia in neurodevelopment. When assessing collective cell migration using the commonly used scratch assay, we did not observe a significant effect of the KIAA0319 knockout (Supplementary Figure 1). However, investigation of single cell migration on soft ERISM substrates showed that single knockout cells move significantly faster than wild type cells (Figure 3C). These contradictory findings can be explained by several factors: the apparent stiffness of the ERISM sensor is in the range of soft tissue (1 to 20 kPa) and significantly different from the stiffness of the cell culture plastic plate

in which the scratch assay was performed (~100,000 kPa) (Skardal et al., 2013). Substrate stiffness has a strong influence on cell migration in vitro (Bangasser et al., 2017). Furthermore, single and collective cell migration are affected by different factors. Finally, while cells respond to an acute event, namely local damage, in the scratch assay, the ERISM assay observes the migration of undisturbed cells. Additionally, ERISM analysis revealed that the knockout cells exert significantly strong forces on their substrate compared to the wild type (Figure 3D). A rescue experiment recovered mechanical activity of the wild type phenotype (Figure 4C) supporting an involvement of KIAA0319 in cellular forces. In addition to the higher cell forces in Ex6KO cells, Ex6KO cells showed stronger temporal oscillation of cell force and migration speed (even though not at a statistically significant level). They also showed more frequent correlated events of high migration speed and a drop in exerted force.

Fluorescent staining revealed the presence of actin-rich spots surrounded by vinculin rings in the studied cell lines (Figure 5). Previously, such local actin cores have been reported to associate with podosomes. By combining fluorescent staining with Fourier-filtered ERISM measurements, we found that the actin cores of podosomes protruded vertically into the substrate, exerting oscillating forces of up to 80 pN, while surrounding rings of pulling sites were tightly colocalised with vinculin. To the best of our knowledge, this is the first report on direct force exertion by podosomes in epithelial cells. WT cells formed podosomes more often than Ex6KO cells.

The link between the functionality of KIAA0319 and the observed phenotypical changes may originate from the molecular structure of the protein. KIAA0319 is a transmembrane protein that contains five PKD domains. These domains have been described in very few human proteins, among which the best characterised is Polycystin-1 (PC1). PC1 acts as a mechanosensor in the membrane of cilia (Dalagiorgou et al., 2010), most probably by unfolding of the highly extensible PKD domains in response to stretching forces. It has been proposed that this unfolding maintains neighbouring cells in contact during cell movement (Qian et al., 2005). PC1 interacts with the cytoskeleton (Boca et al., 2007) and plays an important role in adaptative cilia shortening (for example under strong flow) (Besschetnova et al., 2010). PC1 therefore mediates both cilia length and mechanosensing properties. Our results suggest that KIAA0319 has a similar function to PC1 affecting both cilia formation and mechanosensing. Our data show that knockout of KIAA0319 not only

results in formation of longer cilia, but also in dysregulation of mechanical forces which impairs migration behaviour. We observed that higher cell forces lead to increased fluctuations in the migration pattern, increasing oscillations of cell speed and force. KIAA0319 knockout also results in the formation of fewer podosomes. Podosomes are cell-matrix contacts; their function ranges from cell-matrix adhesion and matrix degradation (facilitating cell invasion) to mechanosensing (Linder & Wiesner, 2016). They are especially prominent in cells of the monocytic lineage but have also been reported in migrating and spreading epithelial cells, where they were found to associate with hemidesmosomes (Spinardi et al., 2004). Hemidesmosomes are adhesive structures specific to epithelial cells that regulate a wide range of biological processes, including among others cell migration, exertion of traction force and mechanosensing (Grashoff et al., 2010; Hiroyasu et al., 2016; Spinardi et al., 2004; Walko et al., 2015; Zhang et al., 2011). Direct measurements of the forces exerted by podosomes in epithelial cells have not been reported in the literature so far and our work shows for the first time that epithelial podosomes mechanically probe the environment by exerting oscillating forces in the pN-range, similarly to what has been previously described for podosomes formed by macrophages (Kronenberg et al., 2017; Labernadie et al., 2014). Podosome formation was reduced in the Ex6KO cells compared to the WT, which suggests an involvement of KIAA0319 in cellular mechanosensing.

While our work shows that knockout of KIAA0319 affects cytoskeleton dynamics, the pathways involved in this regulation are not yet known. Earlier studies have also suggested a link between KIAA0319 function and cytoskeleton regulation. KIAA0319 over-expression inhibits axon growth and KIAA0319 knockout results in neurite outgrowth (Franquinho et al., 2017), two processes controlled by cytoskeleton filaments. Genes with roles in microtubule cytoskeleton function have been found to be associated with other neurodevelopmental disorders including schizophrenia, depression, bipolar disorder (Marchisella et al., 2016) and autism (Lin et al., 2016).

In summary, this study advances our understanding of the cellular function of the KIAA0319 dyslexia susceptibility gene. Our data contributes to the current debate about the role of cell migration and cilia biology in dyslexia, showing that the KIAA0319 is involved in mechanosensation and control of cytoskeletal dynamics. These

processes are likely to play important roles during brain development and may contribute to neurodevelopmental disorders.

Materials and Methods

Cell culture

hTERT-RPE1 cells were generated by transfection with pGRN145, which expresses hTERT under the control of the MPSV promoter, and were kindly supplied by Dr. Andrea Bodnar, Geron Inc. Cell lines were cultured in DMEM F12 with 10% of fetal bovine serum and 1% Penicillin/Streptomycin, or in serum-free media (DMEM F12 with 1% Penicillin/Streptomycin) at 37 °C and 5% CO_2.

Plasmids

pSPgRNA was a gift from Charles Gersbach (Addgene plasmid #47108) (Perez-Pinera et al., 2013). pSPCas9n-2A-GFP (pSpCas9n(BB)-2A-GFP (PX461)) was a gift from Feng Zhang (Addgene plasmid #48140) (Ran et al., 2013). KIAA0319-GFP was a gift from Antonio Velayos-Baeza (Velayos-Baeza et al., 2008).

Cloning and transfection

KIAA0319 knockout cell lines were generated through a CRISPR-Cas9 double nicking strategy designed with the web-based tool developed by Hsu and collaborators (http://crispr.mit.edu) (Hsu et al., 2013). This strategy uses Cas9 nickase (Cas9n), a modified Cas9 in which one of the nuclease domains has been mutated, lowering the rate of off-target effects compared to Cas9 (Ran et al., 2013). RPE1 cells were transfected with pSpCas9n(BB)-2A-GFP (PX461) and paired gRNAs, using Lipofectamine3000 (ThermoFisher). gRNAs were generated by cloning annealed oligonucleotides containing the protospacer sequence into the chimeric gRNA sequence in pSPgRNA linearised with BbsI, downstream of a U6 promoter (Supplementary Table 1). Sequences targeted were AGCCACCCCACAGACTACCA and TAAATTCCATTCATAGTTGT on KIAA0319 exon 6. pSpCas9n(BB)-2A-GFP (PX461) contains a GFP expression cassette that acts as indicator of positive transfection. Twenty-four hours after transfection, 384 individual GFP positive cells (four 96 well plates) were isolated using Fluorescence Activated Cell Sorting (FACS) and plated onto 96 well plates coated with Poly-D-Lysine for clonal expansion.

Screening

Fifty cells were successfully expanded for further analysis. PCR was performed in all clones using primers int6-7R and int5-6F, that amplify a 1311 sequence DNA flanking the site targeted with the gRNAs (Supplementary Table 1). Amplicons were digested with the restriction enzyme StyI. One of the used gRNAs targets this sequence, hence mutations caused by this gRNA are likely to eliminate this site. Amplicons from the 7 clones that showed loss of a StyI site upon digestion were cloned into Zero Blunt TOPO (ThermoFisher K280020) and sequenced using primers SP6 and T7. We identified one of these lines as a homozygous knockout as it contains two types of deletions causing frameshifts and premature stop codons.

Immunofluorescence

Cells on the ERISM micro-cavity were fixed with 4% paraformaldehyde (PFA) in PBS at room temperature for 20 minutes. Immediately after fixation, cells were permeabilised with 0.1%Triton X-100 for 3 minutes and blocked for 30 minutes with 1% BSA in PBS. Cells were then stained for vinculin using anti-vinculin antibody (Merck Millipore, cat. no. 90227, 1:250 in BSA solution, 1 hour at room temperature) and for actin using TRITC-conjugated phalloidin (MerckMillipore, cat. no. 90228, 1:500 in BSA solution, 1 hour at room temperature). The nuclei of the cells were stained with DAPI (MerckMillipore, 1:1,000 in BSA), at room temperature for 3 minutes.

RPE1 cells for cilia analysis were cultured on uncoated coverslips for 24 hours with serum-free media, fixed with 4% PFA for 10 minutes, permeabilised with 0.1%Triton X-100, blocked with 10% goat serum in PBS, and stained with the ciliary marker ARL13B Antibody Rabbit polyclonal (17711-1-AP Proteintech) and anti-gamma-tubulin (Abcam 11316). Under serum starvation, cells stay in G_0 and form cilia. We measured the length of the cilia manually using ImageJ. To ensure that cilia were positioned flat against the surface of the cell, only cilia that were completely in focus were considered.

Gene expression quantification

qRT-PCRs were performed using Luna OneStep reagent (NEB) on biological triplicates. KIAA0319 expression was assessed with primers ex11F and ex12R (Supplementary Table 1). Analysis was performed by the ΔΔCt method using Beta-

actin as endogenous control. Results were normalised against expression in WT cells. Error bars are calculated using the standard deviation of the triplicates ($2^{\Delta\Delta Ct\text{-}s.d}$ - $2^{\Delta\Delta Ct+\text{-}s.d}$).

Western blot

Protein lysates were obtained from all cell lines using RIPA buffer and separated in a NuPAGE Bis-Tris 4-12% gradient gel (ThermoFisher). Proteins were transferred to a nitrocellulose membrane, blocked in WesternBreeze blocker (ThermoFisher) and incubated with primary antibodies anti-GFP (Chromotek #029762) and anti-beta actin (Sigma). Secondary antibodies were donkey anti-rat and anti-mouse HRP conjugated. Membranes were developed using SuperSignal WestFemto substrate (ThermoFisher).

Scratch assay

The scratch assay is a simple way to measure cell migration in vitro and consists on creating a “scratch” on a confluent layer of cells and quantifying the movement of the cells over time to close this gap (Liang et al., 2007). Since this test is performed in serum free culture conditions, which prevent the cells from dividing, it only takes into account cell movement and not proliferation. Wild type and Ex6KO cell lines were plated on a 6-well plate. When confluent, the layer of cells was scratched with a pipette tip creating a straight gap. Cells were then washed with PBS to remove media and floating cells, and serum free media was added. We took images covering the whole gap at the time of the scratch (time 0) and after 24 hours. We measured the width of the scratch using TScratch (Geback et al., 2009), and calculated the mean width for each cell line after 24 hours.

ERISM measurements

ERISM substrates were fabricated as described previously (Kronenberg, 2017) and four silicon chambers (surface area: 0.75 x 0.75 cm^2; Ibidi) were applied. RPE1 cells were seeded on the ERISM substrate at 1,000 cells per well and kept at 37 °C, 5% CO_2 culture conditions in DMEM-12 supplemented with 10% FBS and 1% Penicillin/Streptomycin. WT and Ex6KO cells as well as WT, WT_K-GFP, Ex6KO and Ex6KO_K-GFP cells were investigated in different wells on the same ERISM chip. Prior to ERISM measurements, cells were cultured for 24 h to allow adhesion to

complete. ERISM force measurements were performed and converted into displacement maps as described before (Kronenberg et al., 2017). To investigate forces during cell migration, ERISM maps were recorded continuously for 17 h at intervals of 5 minutes, recording from seven different positions within each of the respective wells with a x20 objective. To analyse the force exertion patterns, ERISM measurements were performed at higher frame rate (every 5 s or 2 min) and magnification (x40 objective). To generate the Fourier-filtered ERISM maps, a FFT bandpass filter was applied to the raw displacement maps using the ImageJ software. For cell force analysis, the volume by which migrating cells indent into the ERISM substrate was calculated using ImageJ. All pixels in the ERISM displacement maps with indentation of less than 20 nm were set to NaN's (not a number) and the "indented volume" under each individual cell was calculated as the product of area and mean indentation. Only cells that moved freely for >4 h (i.e. that were not in physical contact with other cells) were included in the analysis.

The "indentation force" of a single podosome protrusion was calculated by converting spatial Fourier-filtered ERISM displacement maps with a cut-off frequency of 0.6 μm^{-1} into stress maps using FEM as described in Kronenberg, 2017. Podosome protrusions were identified in stress maps as isolated, localised indentation surrounded by a ring of pulling. Indentation force was calculated as the product of indentation area and mean applied stress at a threshold of 4 Pa. Only structures that colocalise with actin-dots in the respective immunostaining image were analysed.

To calculate the "contraction force" of single focal adhesions, the twist in spatial Fourier-filtered ERISM displacement maps with a cut-off frequency of 0.6 μm^{-1} were analysed and converted into the corresponding horizontally exerted contractile forces as described in Kronenberg, 2017. In short, twisting results from the torque applied by focal adhesions when transmitting contractile cell forces to the ERISM substrate. The twisting response of ERISM substrates was calibrated by applying horizontal forces using AFM. The amount of twisting was found to be directly proportional to the applied force (6.6 nm of twist per 1 nN of applied force; $R^2 > 0.99$; $n = 5$ force measurements). Only twists in ERISM displacement maps that form around vinculin-rich areas in the respective immunostaining image were analysed.

The "directness" of cell migration was calculated as the product of euclidean distance and accumulated distance relative to the position of the cell at the start of the measurement. The speed of the cells on the ERISM sensor was measured using the plugin Manual Tracking on ImageJ (Schneider et al., 2012).

Generation of cell lines expressing KIAA0319-GFP

RPE1 wild type and Ex6KO were transfected with linearised KIAA0319-GFP plasmid using Lipofectamine 3000 according to the manufacturer's specifications. KIAA0319-GFP contains a neomycin resistance cassette that was used to select cells that had undergone stable transfection, integrating the construct in their genome. Stably transfected cells were selected with G418 (Roche) at a concentration of 400 µg ml^{-1} for 2 weeks. Cells tend to lose the expression of the transgene with time (Mutskov & Felsenfeld, 2004), and after a few passages of this cell line, GFP expression was detected in only a small percentage of the cells. To enrich cells expressing the construct, we selected GFP positive cells via FACS. After FACS selection, cells were kept in culture for 24 hours to allow them to recover, and then plated onto the ERISM microcavity for measurement.

Acknowledgements

This work was supported by Royal Society [RG160373], Carnegie Trust [50341], Action Medical Research [GN 2614] grants to SP and Engineering and Physical Sciences Research Council [EP/P030017/1], Biotechnology and Biological Sciences Research Council [BB/P027148/1], and the European Research Council Starting Grant ABLASE [640012] grants to MCG. SP is a Royal Society University Research Fellow.

Figures

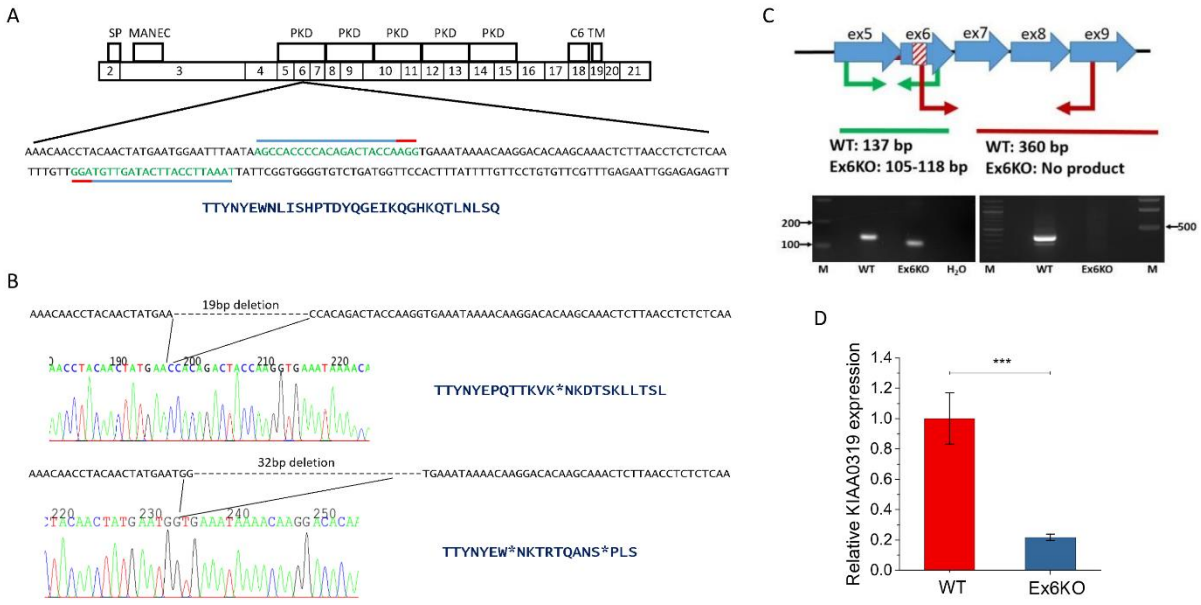

Figure 1: Generation of a cellular KIAA0319 knock out

(A) Top: Structure of Human KIAA0319 (adapted from Velayos-Baeza et al., 2008 and Ensembl release 94 (Zerbino et al., 2018)). The diagram shows the correspondence between protein domains and coding exons in KIAA0319. Signal peptide (SP), MANEC domain (MANEC), PKD domains (PKD), cysteine residues (C6) and transmembrane domain (TM) are indicated. Bottom: full DNA sequence of KIAA0319 exon 6 with target sequences for the gRNAs indicated with blue lines. Red lines show the position of the PAM sequences. Translated sequence of amino acids for the targeted exon is shown below the DNA sequence. **(B)** Chromatograms of the deletions found in Ex6KO and translated corresponding amino acids for wild type and knockout cell line. Asterisks indicate premature stop codons. **(C)** Results of the PCR screening to confirm the deletions in Ex6KO. The cartoon on the left represents the screening strategy. Two sets of primers were designed to give different bands in the WT and KO. The stripped area indicates the 19 and 32 base pair (bp) deletions in the exon 6 of KIAA0319. The first set of primers (Ex_6R and Ex_5F) amplifies the region around the deletion and therefore a smaller band is expected for the KO (105 – 118 bp) compared to the WT (137 bp). The second pair (Ex9_R/Ex6delF) has one primer mapping within the deletion. PCR is expected to give a band of 360 bp in the WT and no product in the KO. Images below confirm the expected results for both pairs. **(D)** Quantification of KIAA0319 mRNA in WT and Ex6KO by qPCR. KIAA0319 expression is significantly lower in Ex6KO (Student's *t*-test: $p < 0.0001$), consistent with nonsense mediated decay of the mRNA caused by the deletion.

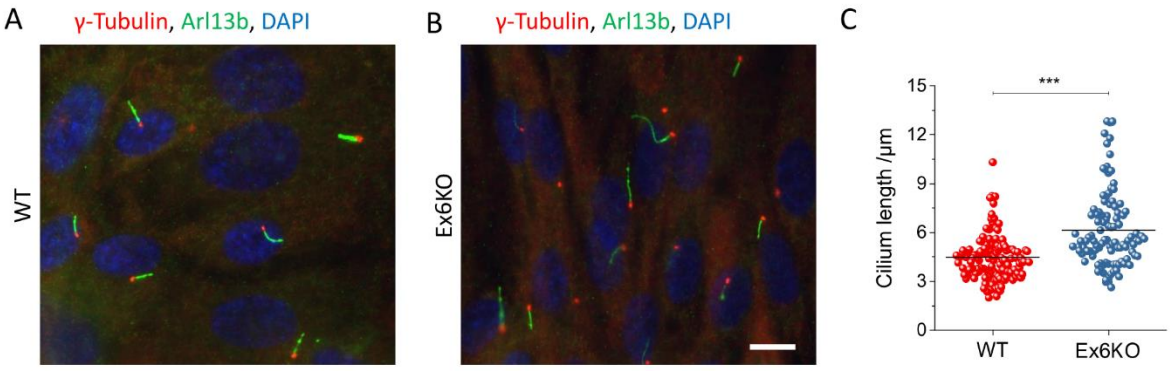

Figure 2: Analysis of the cilia length

Representative immunofluorescence images of RPE1 wild type (**A**) and Ex6KO (**B**), stained for cilia marker Arl13b (green), centrosomal marker γ-tubulin (red), and DAPI (blue). **(C)** Plot of the cilia length for wild type (n = 129) and Ex6KO cells (n = 104). Groups were compared using the Student's t-test (***$p < 0.001$). Scale bar, 10 µm.

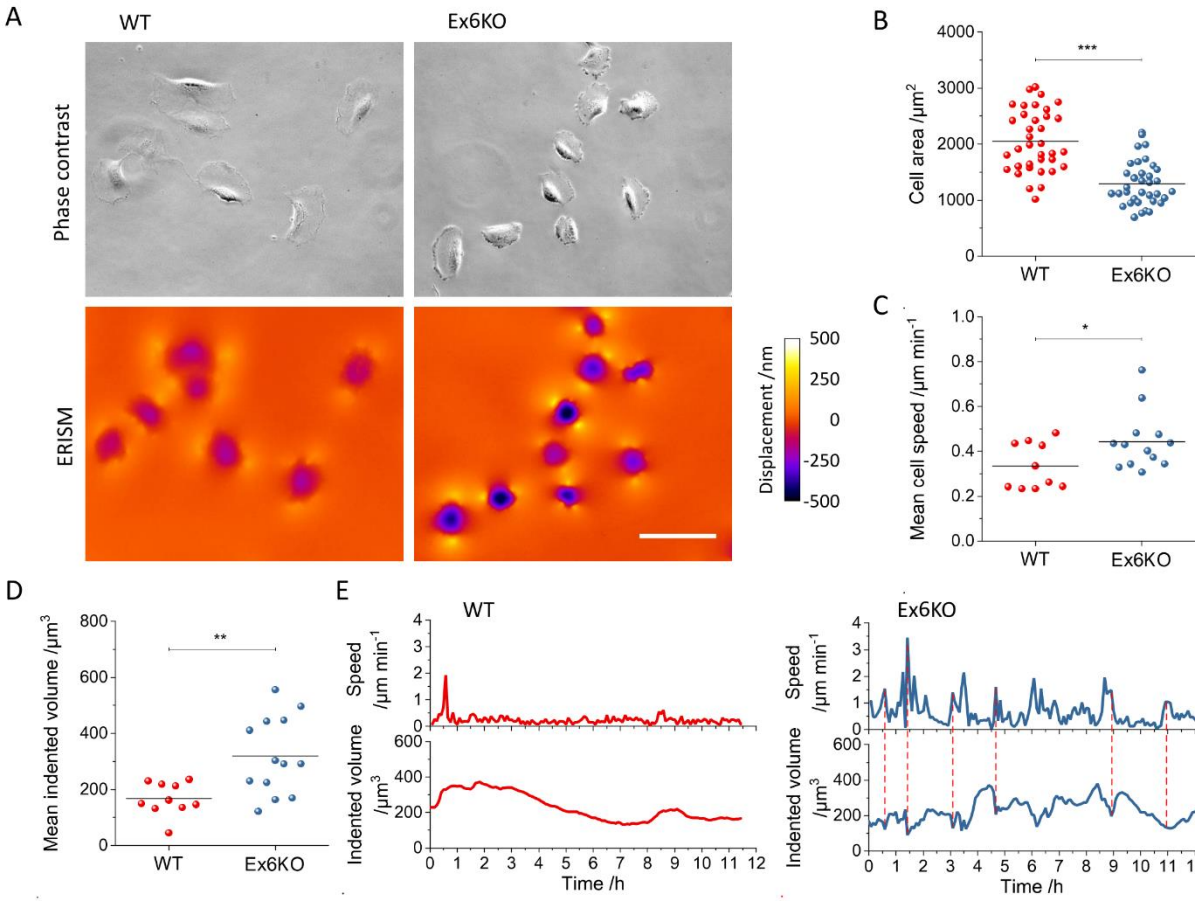

Figure 3: Analysis of mechanical activity of RPE1 WT and Ex6KO cells during migration on an ERISM micro-cavity

(A) Phase contrast (upper row) and ERISM micro-cavity displacement maps (lower row) of WT (left) and Ex6KO (right) cells. **(B)** Comparison of the surface area covered by WT (*n* = 36) and Ex6KO (*n* = 36) cells types. **(C)** Comparison of mean speed of WT (*n* = 10) and Ex6KO (*n* = 13) cells. **(D)** Comparison of mean indented volume of WT (*n* = 10) and Ex6KO (*n* = 13) cells. Only cells with free movement for >4 h were included in analysis of speed and indented volume. Plots in (B), (D) and (E) show all measured data points and the mean (line). Groups were compared using the Student's *t*-test (**p* <0.05, ***p* <0.01, ****p* <0.001). **(E)** Exemplary temporal evolution of speed and mechanical activity (using the total volume by which each cell indents into the ERISM substrate as a proxy for the applied force) of representative RPE1 WT (left panel) and Ex6KO (right panel) cells, following the movement of two individual cells on an ERISM micro-cavity for >11 h. Red, vertical lines indicate timepoints when high migration speed of Ex6KO cells correlate with a drop in exerted force. Scale bar, 50 µm.

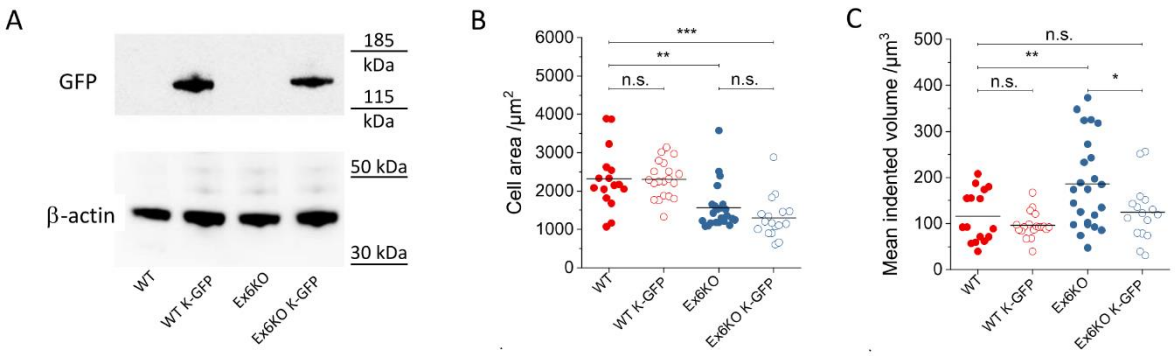

Figure 4: Phenotype recovery through KIAA0319 rescue

(A) Western blot confirming the presence of a fusion protein (140 KDa) following transfection with a full length KIAA0319 construct fused to a GFP tag. **(B)** Comparison of area covered by RPE1 WT, WT K-GFP, Ex6KO and Ex6KO K-GFP cells attached to ERISM micro-cavity. (WT: n = 16, WT K-GFP: n = 20, Ex6KO: n = 23, Ex6KO K-GFP: n = 17) **(C)** Comparison of mean mechanical activity of RPE1 WT, WT K-GFP, Ex6KO and Ex6KO K-GFP cells during migration on ERISM micro-cavity. Only cells with free movement for >4 h were included in the analysis. Plots in B and C show measured data points and the mean (line). (WT: n = 16, WT K-GFP: n = 19, Ex6KO: n = 24, Ex6KO K-GFP: n = 16) Groups were compared using the Student's t-test (*p < 0.05, **p < 0.01, ***p < 0.001).

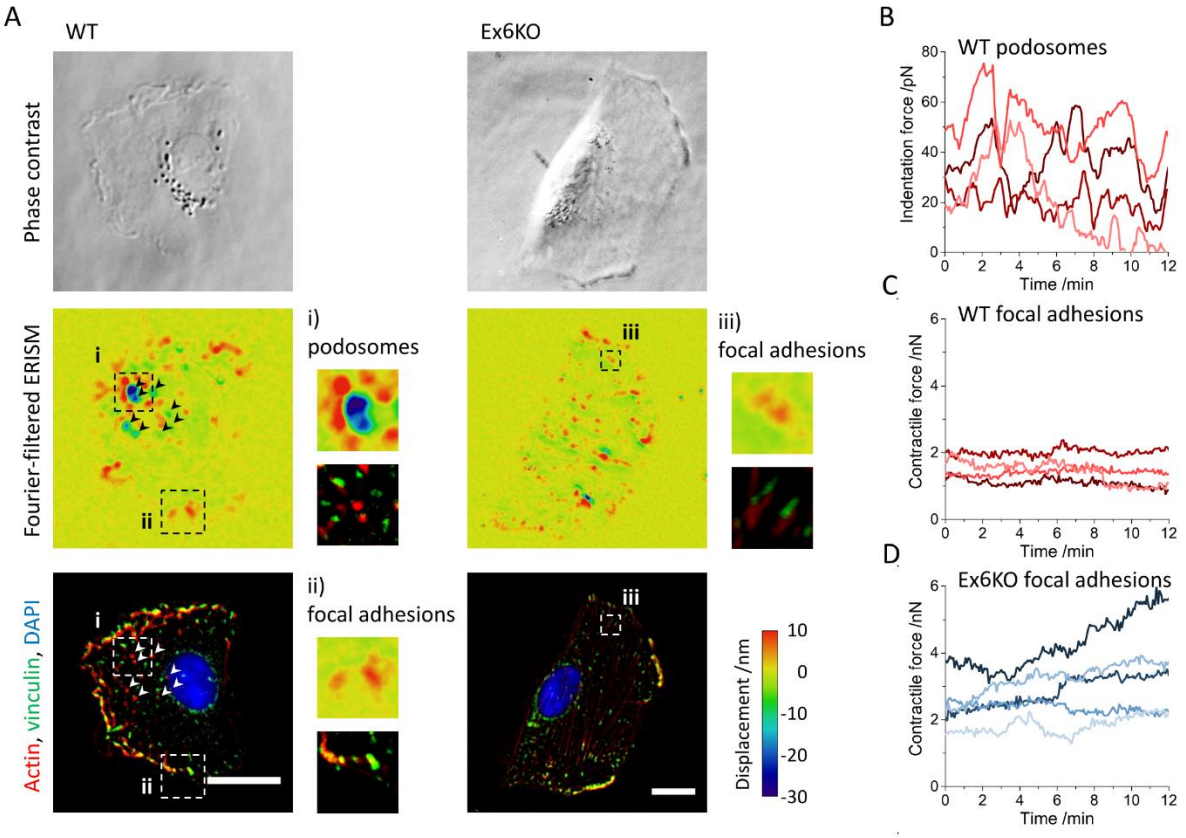

Figure 5: RPE1 KIAA0319 WT and Ex6KO cells use different modes of force exertion **(A)** Phase contrast images (upper row), Fourier-filtered ERISM displacement maps (middle row) and epi-fluorescence images (lower row, red: actin, green: vinculin, blue: nuclear DNA) of a RPE1 WT cell (left column) and an Ex6KO cell (right column). Arrow heads indicate positions of actin-rich cell protrusions (podosomes). The insets i) in the Fourier-filtered ERISM map and the epi-fluorescence image of the WT cell show magnifications of podosome protrusions. The insets ii) and iii) show magnifications of vinculin-rich cell-substrate contacts (focal adhesions) for the WT and Ex6KO cell, respectively. **(B)** Temporal evolution of the indentation force applied by different podosomes of the WT cell shown in A. **(C)** and **(D)** Temporal evolution of the contraction force applied by different focal adhesions of the WT and Ex6KO cell shown in A, respectively. All scale bars: 20 µm.

References

Avasthi, P., & Marshall, W. F. (2012). Stages of ciliogenesis and regulation of ciliary length. *Differentiation*, *83*, S30–S42.

Baek, S. T., Kerjan, G., Bielas, S. L., Lee, J. E., Fenstermaker, A. G., Novarino, G., & Gleeson, J. G. (2014). Off-target effect of doublecortin family shRNA on neuronal migration associated with endogenous MicroRNA dysregulation. *Neuron*, *82*(6), 1255–1262.

Baker, K. E., & Parker, R. (2004). Nonsense-mediated mRNA decay: terminating erroneous gene expression. *Current Opinion in Cell Biology*, *16*(3), 293–299.

Bangasser, B. L., Shamsan, G. A., Chan, C. E., Opoku, K. N., Tüzel, E., Schlichtmann, B. W., Kasim, J. A., Fuller, B. J., McCullough, B. R., Rosenfeld, S. S., & Odde, D. J. (2017). Shifting the optimal stiffness for cell migration. *Nature Communications*, *8*, 15313.

Besschetnova, T. Y., Kolpakova-Hart, E., Guan, Y., Zhou, J., Olsen, B. R., & Shah, J. V. (2010). Identification of Signaling Pathways Regulating Primary Cilium Length and Flow-Mediated Adaptation. *Current Biology*, *20*(2), 182–187.

Boca, M., D'amato, L., Distefano, G., Polishchuk, R. S., Germino, G. G., & Boletta, A. (2007). Polycystin-1 Induces Cell Migration by Regulating Phosphatidylinositol 3-kinase-dependent Cytoskeletal Rearrangements and GSK3-dependent Cell-Cell Mechanical Adhesion. *Molecular Biology of the Cell*, *18*, 4050–4061.

Brandler, W. M., & Paracchini, S. (2013). The genetic relationship between handedness and neurodevelopmental disorders. *Trends in Molecular Medicine*, 1–8.

Bycroft, M., Bateman, A., Clarke, J., Hamill, S. J., Sandford, R., Thomas, R. L., & Chothia, C. (1999). The structure of a PKD domain from polycystin-1: Implications for polycystic kidney disease. *EMBO Journal*, *18*(2), 297–305.

Centanni, T. M., Booker, A. B., Sloan, A. M., Chen, F., Maher, B. J., Carraway, R. S., Khodaparast, N., Rennaker, R., LoTurco, J. J., & Kilgard, M. P. (2014). Knockdown of the dyslexia-associated gene Kiaa0319 impairs temporal responses to speech stimuli in rat primary auditory cortex. *Cerebral Cortex*, *24*(7), 1753–1766.

Centanni, T. M., Chen, F., Booker, A. M., Engineer, C. T., Sloan, A. M., Rennaker, R. L., LoTurco, J. J., & Kilgard, M. P. (2014). Speech Sound Processing Deficits and Training-Induced Neural Plasticity in Rats with Dyslexia Gene Knockdown. *PLoS ONE*, *9*(5),

e98439.

Chandrasekar, G., Vesterlund, L., Hultenby, K., Tapia-Páez, I., & Kere, J. (2013). The zebrafish orthologue of the dyslexia candidate gene DYX1C1 is essential for cilia growth and function. *PloS One*, *8*(5), e63123.

Dalagiorgou, G., Basdra, E. K., & Papavassiliou, A. G. (2010). Polycystin-1: Function as a mechanosensor. *The International Journal of Biochemistry & Cell Biology*, *42*(10), 1610–1613.

Franquinho, F., Nogueira-Rodrigues, J., Duarte, J. M., Esteves, S. S., Carter-Su, C., Monaco, A. P., Molnár, Z., Velayos-Baeza, A., Brites, P., & Sousa, M. M. (2017). The Dyslexia-susceptibility Protein KIAA0319 Inhibits Axon Growth Through Smad2 Signaling. *Cerebral Cortex*, *27*(3), 1732–1747.

Galaburda, A. M. (2018). The Role of Rodent Models in Dyslexia Research: Understanding the Brain, Sex Differences, Lateralization, and Behavior. In T. Lachmann & T. Weis (Eds.), *Reading and Dyslexia: From Basic Functions to Higher Order Cognition* (pp. 77–96). Cham: Springer International Publishing.

Galaburda, A. M., Sherman, G. F., Rosen, G. D., Aboitz, F., & Geschwind, N. (1985). Developmental Dyslexia: Four consecutive patients with cortical anomaly. *Annals of Neurology*, *18*(2), 222–223.

Geback, T., Schulz, M. M. P., Koumoutsakos, P., & Detmar, M. (2009). TScratch: A novel and simple software tool for automated analysis of monolayer wound healing assays. *BioTechniques*, *46*(4), 265–274.

Geremek, M., Ziętkiewicz, E., Bruinenberg, M., Franke, L., Pogorzelski, A., Wijmenga, C., & Witt, M. (2014). Ciliary genes are down-regulated in bronchial tissue of primary ciliary dyskinesia patients. *PLoS ONE*, *9*(2).

Gostic, M., Martinelli, A., Tucker, C., Yang, Z., Ewart, F. G. J., Dholakia, K., Sillar, K. T., Tello, J. A., & Paracchini, S. (2019). The dyslexia susceptibility KIAA0319 gene shows a specific expression pattern during zebrafish development supporting a role beyond neuronal migration. *Journal of Comparative Neurology*, 1–10.

Grashoff, C., Hoffman, B. D., Brenner, M. D., Zhou, R., Parsons, M., Yang, M. T., McLean, M. A., Sligar, S. G., Chen, C. S., Ha, T., & Schwartz, M. A. (2010). Measuring mechanical tension across vinculin reveals regulation of focal adhesion dynamics. *Nature*, *466*(7303), 263–266.

632 Grati, M., Chakchouk, I., Ma, Q., Bensaid, M., Desmidt, A., Turki, N., Yan, D., Baanannou,
633 A., Mittal, R., Driss, N., Blanton, S., Farooq, A., Lu, Z., Liu, X. Z., & Masmoudi, S.
634 (2015). A missense mutation in DCDC2 causes human recessive deafness DFNB66,
635 likely by interfering with sensory hair cell and supporting cell cilia length regulation.
636 *Human Molecular Genetics*, *24*(9), 2482–2491.

637 Guidi, L. G., Mattley, J., Martinez-Garay, I., Monaco, A. P., Linden, J. F., Velayos-Baeza, A.,
638 & Molnár, Z. (2017). Knockout Mice for Dyslexia Susceptibility Gene Homologs
639 KIAA0319 and KIAA0319L have Unaffected Neuronal Migration but Display Abnormal
640 Auditory Processing. *Cerebral Cortex*, *27*(12), 5831–5845.

641 Guidi, L. G., Velayos-Baeza, A., Martinez-Garay, I., Monaco, A. P., Paracchini, S., Bishop,
642 D. V. M., & Molnár, Z. (2018). The Neuronal Migration Hypothesis of Dyslexia: A Critical
643 Evaluation Thirty Years On. *European Journal of Neuroscience*, (48), 3212–3233.

644 Higginbotham, H., Eom, T.-Y., Mariani, L. E., Bachleda, A., Hirt, J., Gukassyan, V., Cusack,
645 C. L., Lai, C., Caspary, T., & Anton, E. S. (2012). Arl13b in primary cilia regulates the
646 migration and placement of interneurons in the developing cerebral cortex.
647 *Developmental Cell*, *23*(5), 925–38.

648 Hiroyasu, S., Colburn, Z. T., & Jones, J. C. R. (2016). A hemidesmosomal protein regulates
649 actin dynamics and traction forces in motile keratinocytes. *FASEB Journal*, *30*(6),
650 2298–2310.

651 Hoh, R. a, Stowe, T. R., Turk, E., & Stearns, T. (2012). Transcriptional program of ciliated
652 epithelial cells reveals new cilium and centrosome components and links to human
653 disease. *PloS One*, *7*(12), e52166.

654 Hsu, P. D., Scott, D. A., Weinstein, J. A., Ran, F. A., Konermann, S., Agarwala, V., Li, Y.,
655 Fine, E. J., Wu, X., Shalem, O., Cradick, T. J., Marraffini, L. A., Bao, G., & Zhang, F.
656 (2013). DNA targeting specificity of RNA-guided Cas9 nucleases. *Nature*
657 *Biotechnology*, *31*(9), 827–832.

658 Hughes, J., Ward, C. J., Peral, B., Aspinwall, R., Clark, K., San Millan, J. L., Gamble, V., &
659 Harris, P. C. (1995). The polycystic kidney disease 1 (PKD1) gene encodes a novel
660 protein with multiple cell recognition domains. *Nature*, *10*, 151–160.

661 Ibraghimov-Beskrovnaya, O., Bukanov, N. O., Donohue, L. C., Dackowski, W. R., Klinger, K.
662 W., & Landes, G. M. (2000). Strong homophilic interactions of the Ig-like domains of
663 polycystin-1, the protein product of an autosomal dominant polycystic kidney disease
664 gene, PKD1. *Human Molecular Genetics*, *9*(11), 1641–9.

Ivliev, A. E., 't Hoen, P. a C., van Roon-Mom, W. M. C., Peters, D. J. M., & Sergeeva, M. G. (2012). Exploring the transcriptome of ciliated cells using in silico dissection of human tissues. *PloS One*, *7*(4), e35618.

Kim, J., Jo, H., Hong, H., Kim, M. H., Kim, J. M., Lee, J.-K., Heo, W. Do, & Kim, J. (2015). Actin remodelling factors control ciliogenesis by regulating YAP/TAZ activity and vesicle trafficking. *Nature Communications*, *6*, 6781.

Kronenberg, N. M., Liehm, P., Steude, A., Knipper, J. A., Borger, J. G., Scarcelli, G., Franze, K., Powis, S. J., & Gather, M. C. (2017). Long-term imaging of cellular forces with high precision by elastic resonator interference stress microscopy. *Nature Cell Biology*, *19*(7), 864–872.

Labernadie, A., Bouissou, A., Delobelle, P., Balor, S., Voituriez, R., Proag, A., Fourquaux, I., Thibault, C., Vieu, C., Poincloux, R., Charrière, G. M., & Maridonneau-Parini, I. (2014). Protrusion force microscopy reveals oscillatory force generation and mechanosensing activity of human macrophage podosomes. *Nature Communications*, *5*, 5343.

Legant, W. R., Choi, C. K., Miller, J. S., Shao, L., Gao, L., Betzig, E., & Chen, C. S. (2013). Multidimensional traction force microscopy reveals out-of-plane rotational moments about focal adhesions. *Proceedings of the National Academy of Sciences*, *110*(3), 1–6.

Liang, C. C., Park, A. Y., & Guan, J. L. (2007). In vitro scratch assay: a convenient and inexpensive method for analysis of cell migration in vitro. *Nature Protocols*, *2*(2), 329–333.

Liehm, P., Kronenberg, N. M., & Gather, M. C. (2018). Analysis of the Precision, Robustness, and Speed of Elastic Resonator Interference Stress Microscopy. *Biophysical Journal*, (114), 2180–2193.

Lin, Y.-C., Frei, J. A., Kilander, M. B. C., Shen, W., & Blatt, G. J. (2016). A Subset of Autism-Associated Genes Regulate the Structural Stability of Neurons. *Frontiers in Cellular Neuroscience*, *10*, 263.

Linder, S., & Wiesner, C. (2016). Feel the force: Podosomes in mechanosensing. *Experimental Cell Research*, *343*(1), 67–72.

Marchisella, F., Coffey, E. T., & Hollos, P. (2016). Microtubule and microtubule associated protein anomalies in psychiatric disease. *Cytoskeleton*, *73*(10), 596–611.

Martinez-Garay, I., Guidi, L. G., Holloway, Z. G., Bailey, M. A. G., Lyngholm, D., Schneider, T., Donnison, T., Butt, S. J. B., Velayos-Baeza, A., Molnár, Z., & Monaco, A. P. (2016).

Normal radial migration and lamination are maintained in dyslexia-susceptibility candidate gene homolog Kiaa0319 knockout mice. *Brain Structure and Function*, *222*(3), 1367–1384.

Massinen, S., Hokkanen, M.-E., Matsson, H., Tammimies, K., Tapia-Páez, I., Dahlström-Heuser, V., Kuja-Panula, J., Burghoorn, J., Jeppsson, K. E., Swoboda, P., Peyrard-Janvid, M., Toftgård, R., Castrén, E., & Kere, J. (2011). Increased expression of the dyslexia candidate gene DCDC2 affects length and signaling of primary cilia in neurons. *PloS One*, *6*(6), e20580.

Mutskov, V., & Felsenfeld, G. (2004). Silencing of transgene transcription precedes methylation of promoter DNA and histone H3 lysine 9. *The EMBO Journal*, *23*(1), 138–49.

Newbury, D. F., Monaco, A. P., & Paracchini, S. (2014). Reading and language disorders: the importance of both quantity and quality. *Genes*, *5*(2), 285–309.

Paracchini, S., Diaz, R., & Stein, J. (2016). *Advances in Dyslexia Genetics—New Insights Into the Role of Brain Asymmetries*. *Advances in Genetics* (Vol. 96). Elsevier Ltd.

Paracchini, S., Scerri, T., & Monaco, A. P. (2007). The genetic lexicon of dyslexia. *Annual Review of Genomics and Human Genetics*, *8*, 57–79.

Perez-Pinera, P., Kocak, D. D., Vockley, C. M., Adler, A. F., Kabadi, A. M., Polstein, L. R., Thakore, P. I., Glass, K. A., Ousterout, D. G., Leong, K. W., Guilak, F., Crawford, G. E., Reddy, T. E., & Gersbach, C. A. (2013). RNA-guided gene activation by CRISPR- Cas9 – based transcription factors. *Nature Methods*, *10*(10), 973–976.

Peterson, R. L., & Pennington, B. F. (2012). Developmental dyslexia. *The Lancet*, *379*(9830), 1997–2007.

Pugacheva, E. N., Jablonski, S. A., Hartman, T. R., Henske, E. P., & Golemis, E. A. (2007). HEF1-Dependent Aurora A Activation Induces Disassembly of the Primary Cilium. *Cell*, *129*(7), 1351–1363.

Qian, F., Wei, W., Germino, G., & Oberhauser, A. (2005). The nanomechanics of polycystin-1 extracellular region. *The Journal of Biological Chemistry*, *280*(49), 40723–30.

Ran, F. A., Hsu, P. D., Wright, J., Agarwala, V., Scott, D. a, & Zhang, F. (2013). Genome engineering using the CRISPR-Cas9 system. *Nature Protocols*, *8*(11), 2281–308.

Rendall, A. R., Tarkar, A., Contreras-Mora, H. M., Loturco, J. J., & Fitch, R. H. (2015). Deficits in learning and memory in mice with a mutation of the candidate dyslexia

susceptibility gene Dyx1c1. *Brain and Language*, *172*, 30–38.

Rossi, A., Kontarakis, Z., Gerri, C., Nolte, H., Hölper, S., Krüger, M., & Stainier, D. Y. R. (2015). Genetic compensation induced by deleterious mutations but not gene knockdowns. *Nature*, *Aug 13*(524), 230–3.

Schindelin, J., Arganda-Carreras, I., Frise, E., Kaynig, V., Longair, M., Pietzsch, T., Preibisch, S., Rueden, C., Saalfeld, S., Schmid, B., Tinevez, J.-Y., White, D. J., Hartenstein, V., Eliceiri, K., Tomancak, P., & Cardona, A. (2012). Fiji: an open-source platform for biological-image analysis. *Nature Methods*, *9*(7), 676–682.

Schneider, C. A., Rasband, W. S., & Eliceiri, K. W. (2012). NIH Image to ImageJ: 25 years of image analysis. *Nature Methods*, *9*(7), 671–675.

Schueler, M., Braun, D. A., Chandrasekar, G., Gee, H. Y., Klasson, T. D., Halbritter, J., Bieder, A., Porath, J. D., Airik, R., Zhou, W., LoTurco, J. J., Che, A., Otto, E. A., Böckenhauer, D., Sebire, N. J., Honzik, T., Harris, P. C., … Hildebrandt, F. (2015). DCDC2 Mutations Cause a Renal-Hepatic Ciliopathy by Disrupting Wnt Signaling. *The American Journal of Human Genetics*, *96*(1), 81–92.

Skardal, A., Mack, D., Atala, A., & Soker, S. (2013). Substrate elasticity controls cell proliferation , surface marker expression and motile phenotype in amniotic fluid-derived stem cells. *Journal of the Mechanical Behavior of Biomedical Materials*, *17*, 307–316.

Spinardi, L., Rietdorf, J., Nitsch, L., Bono, M., Tacchetti, C., Way, M., & Marchisio, P. C. (2004). A dynamic podosome-like structure of epithelial cells. *Experimental Cell Research*, *295*(2), 360–374.

Szalkowski, C. E., Fiondella, C. G., Galaburda, A. M., Rosen, G. D., LoTurco, J. J., & Fitch, R. H. (2012). Neocortical disruption and behavioral impairments in rats following in utero RNAi of candidate dyslexia risk gene Kiaa0319. *International Journal of Developmental Neuroscience*, *30*(4), 293–302.

Tallal, P. (1980). Auditory temporal perception, phonics, and reading disabilities in children. *Brain and Language*, *9*(2), 182–198.

Tarkar, A., Loges, N. T., Slagle, C. E., Francis, R., Dougherty, G. W., Tamayo, J. V, Shook, B., Cantino, M., Schwartz, D., Jahnke, C., Olbrich, H., Werner, C., Raidt, J., Pennekamp, P., Abouhamed, M., Hjeij, R., Köhler, G., … Omran, H. (2013). DYX1C1 is required for axonemal dynein assembly and ciliary motility. *Nature Genetics*, *45*(9), 995–1003.

761 Threlkeld, S. W., McClure, M. M., Bai, J., Wang, Y., LoTurco, J. J., Rosen, G. D., & Fitch, R.
762 H. (2007). Developmental disruptions and behavioral impairments in rats following in
763 utero RNAi of Dyx1c1. *Brain Research Bulletin*, *71*(5), 508–514.

764 Truong, D. T., Che, A., Rendall, A. R., Szalkowski, C. E., Loturco, J. J., Galaburda, A. M., &
765 Holly Fitch, R. (2014). Mutation of Dcdc2 in mice leads to impairments in auditory
766 processing and memory ability. *Genes, Brain and Behavior*, *13*(8), 802–811.

767 Velayos-Baeza, A., Levecque, C., Kobayashi, K., Holloway, Z. G., & Monaco, A. P. (2010).
768 The dyslexia-associated KIAA0319 protein undergoes proteolytic processing with
769 {gamma}-secretase-independent intramembrane cleavage. *The Journal of Biological*
770 *Chemistry*, *285*(51), 40148–62.

771 Velayos-Baeza, A., Toma, C., da Roza, S., Paracchini, S., & Monaco, A. P. (2007).
772 Alternative splicing in the dyslexia-associated gene KIAA0319. *Mammalian Genome*,
773 *18*(9), 627–34.

774 Velayos-Baeza, A., Toma, C., Paracchini, S., & Monaco, A. P. (2008). The dyslexia-
775 associated gene KIAA0319 encodes highly N- and O-glycosylated plasma membrane
776 and secreted isoforms. *Human Molecular Genetics*, *17*(6), 859–71.

777 Walko, G., Castañón, M. J., & Wiche, G. (2015). Molecular architecture and function of the
778 hemidesmosome. *Cell and Tissue Research*, *360*(2), 363–378.

779 Wang, Y., Yin, X., Rosen, G., Gabel, L., Guadiana, S. M., Sarkisian, M. R., Galaburda, A.
780 M., & Loturco, J. J. (2011). Dcdc2 knockout mice display exacerbated developmental
781 disruptions following knockdown of doublecortin. *Neuroscience*, *190*, 398–408.

782 Zerbino, D. R., Achuthan, P., Akanni, W., Ridwan Amode, M., Barrell, D., Bhai, J., Billis, K.,
783 Cummins, C., Gall, A., García, C., García Girón, C., Gil, L., Gordon, L., Haggerty, L.,
784 Haskell, E., Hourlier, T., Izuogu, O. G., Janacek, S.H., Juettemann, T.,Kiang To, J.,
785 Laird, M.R., Lavidas, I., Liu, Z., Loveland, J.E., Maurel, T., Mclaren, W., Moore, B.,
786 Mudge, J., Murphy, D.N., Newman, V., Nuhn, M., Ogeh, D., Ong, C. K., Parker, A.,
787 Patricio, M., Riat, H.S., Schuilenburg, H., Sheppard, D., Sparrow, H., Taylor, K.,
788 Thormann, A., Vullo, A., Walts, B., Zadissa, A., Frankish, A.,Hunt, S.E., Kostadima, M.,
789 Langridge, N., Martin, F.J., Muffato, M., Perry, E., Ruffier, M., Staines, D.M., Trevanion,
790 S.J., Aken, B.L., Cunningham, F., Yates, A., Flicek, P. (2018). Ensembl 2018. *Nucleic*
791 *Acids Research*, *46*.

792 Zhang, H., Landmann, F., Zahreddine, H., Rodriguez, D., Koch, M., & Labouesse, M. (2011).
793 A tension-induced mechanotransduction pathway promotes epithelial morphogenesis.

794 *Nature*, *471*(7336), 99–103.

795